Barite and gypsum precipitation in chalk: A numerical simulation approach revealing the coupled impact of physical and chemical heterogeneities in porous media

A. Rajyaguru, Nicolas Seigneur, O. Bildstein, S. Savoye, Charles Wittebroodt, E.L. Hôpital, V. Detilleux, P. Arnoux, Vincent Lagneau

Barite and gypsum precipitation in chalk: A numerical simulation approach revealing the coupled nature impact of physical and chemical heterogeneities in porous media

Authors:

A. Rajyaguru[1,2], N. Seigneur[2], O.Bildstein[3],S.Savoye[1], C. Wittebroodt[4], E. L.'HÔPITAL[4], V. Detilleux[5], P.Arnoux[1], V. Lagneau[2]*

(1) Université Paris-Saclay, CEA, Service d'Etude du Comportement des Radionucléides (SECR), , Gif-sur-Yvette

(2) Centre de Géosciences, MINES ParisTech, PSL Research University, Paris, France

(3) CEA, DES, IRESNE, DTN, Laboratory for Modeling of Transfers in the Environment, Saint Paul-lez-Durance, France

(4) IRSN, LETIS, Fontenay Aux Roses, France

(5) Bel V, Belgium

Corresponding author address: ashish.rajyaguru@psi.ch

Abstract

In studies relevant to contaminant transport in geosphere, evolution of local physicochemical processes imparts potential challenges in safety and critical assessment issues. The transport of such contaminants in a rock pore structure could occur under advective or diffusive regime. Such transport over spatial and temporal scale depends upon coupling between physical properties of pore structure (permeability, pore size distribution, porosity) and chemical properties of dissolved ionic species (pH, ionic strength, and surface interactions). The nature of such interactions leads to generation of local imbalances in pore solution and enhances dissolution and precipitation of minerals. To predict occurrence of such processes over large spatial and temporal scales, it is imperative to demonstrate how the physical and chemical processes interact within the heterogeneous porous media. In this context, numerical simulations were conducted to model the results of experimental dataset investigating barite and gypsum precipitation in chalk. In the experimental approach, the selected two minerals are end-members of the sulfate-alkali family and exhibit large differences in kinetic rate and solubility, and the reference chalk sample resembles heterogeneity in its pore structure. The numerical simulations revealed that at 1D scale, it was possible to model overall experimental observations at boundary monitoring points such as chemistry evolution in reservoirs, porosity loss during barite and gypsum precipitation, total amount of barite and gypsum in clogging zone and threshold saturation index to initiate precipitation. However, these simulations could not validate the experimentally observed impact of barite and gypsum clogging on changes in water tracer transport. The underlying reasons for such behavior was the formation of a unique clogging zone due to barite and gypsum precipitation. We show that 2D simulations incorporating spatial heterogeneity are able to reproduce the observed precipitation patterns, both for the barite and gypsum experiments. Through 1D and 2D numerical results, we demonstrate the capability of a reactive transport model to validate experimentally observed barite and gypsum precipitation behavior in chalk sample. Furthermore, it also highlights the interplays between physicochemical heterogeneities, mineral reactivity and transport rates which are responsible for the precipitation pattern of the precipitates, and hence their impacts on transport properties.

1 Introduction

Contaminant migration in geological formations over large spatial and temporal scales is mainly governed by reactive transport phenomena. Over time, these contaminants could interact with rock pore structures and due to their physicochemical nature they could generate a local imbalance in existing pH and ionic concentration of rock pore solution. Thus, these local imbalances would result in dissolution of the cemented rock minerals or formation of secondary mineral species via precipitation phenomena. Indeed, these secondary processes would modify the existing pore structure and therefore the transport properties of the rock. For safety and risk analysis, the evolution of such processes over larger temporal and spatial scales could impose conditions where migration of some radiotoxic elements is enhanced and with a possibility of their leaking into nearby important drinking water sources (Moldovan et al., 2003; Thakur et al., 2010).

One such study concerning reactive transport in porous media deals with the trapping of atmospheric CO_2 (global carbon sequestration or GCS) into the rock pore space (Berthe, 2012; Jun et al., 2013; Snæbjörnsdóttir et al., 2020). The sites selected for such concept contains a porous and permeable rock that could easily trap injected CO_2 within its pore space. Indeed, a layer of impervious cap-rock that potentially limits any ionic transport into the surrounding biosphere covers this permeable rock. However, over long term the trapped CO_2 would gradually interact with the cap-rock and modify its local pore chemistry. These changes would trigger dissolution and precipitation of halite, sulfate- or carbonate-bearing minerals that would change cap-rock pore structure and alter its existing sealing properties. Under such scenario, the transport behavior of some ionic species that are trapped in both reservoir and sealing rock is altered and a potential risk is generated of their leak into the surrounding biosphere. Similarly, such secondary process over long times scales could also occur in deep geological host facilities capable for confining long-lived intermediate and high-level radioactive waste (Bradbury et al., 2014). For example, the degradation of cement structures, corrosion of steel assemblies and release of ionic species as fission products would result in generation of chemically active saline or alkaline plumes. Similar to CO_2 sequestration sites, these plumes could interact with cap rock and modify its intact transport properties. In this case, it could leak radiotoxic ions into surrounding biosphere and generate safety issues. Thus, to evaluate the long-term durability of deep geological disposal sites, it is imperative to obtain a robust understanding of the occurrence of such physicochemical processes and their impact on the properties of host rock as well as sealing rock over larger temporal and spatial scales.

Over the years, the understanding of solute transport in geosphere is built upon lab-scale or field scale experimental observations, combined with numerical simulations using geochemical models based on a continuum approach (Bear, 2013; Glaus et al., 2020; Lagneau, 2013; Landesman et al., 2018; Seigneur et al., 2019). The advantage of using such numerical models lies on the representation of the volume of interest as representative elementary volumes (REV) that characterize the local properties of the material such as porosity, diffusivity, permeability, etc. Using this assumption it is possible to simplify the natural but complex geometry of the material at 1D or 2D (homogenized) and to simulate its evolution on large time and space scales. In such models, minerals constituting a selected natural porous material are described in volume fractions and total porosity is the void space between these minerals. A multicomponent reactive fluid containing selected ions of interest is allowed to migrate through these void spaces. From experimental observations, one could

now fix the initial and boundary conditions in the numerical simulations and observe the evolution of dominant physicochemical processes on selected spatial and temporal scale. In this model the dominant processes such as mineral dissolution or precipitation are modeled via classical kinetic rate law in which key input parameters such as kinetic rate constant, saturation index, reactive surface area are obtained from existing thermodynamic database in literature (Lasaga, 2014). Finally, the formation of new void spaces and their feedback on transport properties (permeability, local porosity, diffusivity) are modeled using empirical relationships such as Kozeny-Carman and Archie's relationships (Archie, 1942; Carman, 1937). However, recent studies have shown that formation of secondary mineral is dependent on local pore chemistry and plays an important role in development of overall clogging zone and thereby changes on overall rock transport properties (Sabo and Beckingham, 2021; Seigneur et al., 2019; Steinwinder and Beckingham, 2019).

109109

Thus, replacement of such empirical relationships is complex because rock pore matrix contains multiscale physical and chemical properties such as pore size distributions, surface charge, surface roughness, reactive/non-reactive phases, local precipitation/dissolution rate, pore pressure effect, and varying mineral solubility. In reality, rocks or porous soils may contain such physicochemical spatial properties from micron-size pore scale to submillimeter scale to the basin scale and their coupling further control the interplay between mass transport and reaction kinetics, creating altered zones favoring precipitation/dissolution(Berkowitz et al., 2006; Bruns et al., 2017; Noiriel et al., 2021; Trinchero and Iraola, 2020). Thus, it is imperative to investigate local reaction kinetics and the corresponding mass transport changes at pore scale for diverse range of porous materials and minerals relevant of geochemistry for the development of new feedback relationships that could replace the existing Archie's or Kozeny-Carman relationships (Nooraiepour et al., 2021; Steefel and Yang, 2021; Varzina et al., 2020).

In this view, the aim of this study is to investigate numerically the impact of mineral intrinsic properties (solubility, precipitation rate, nucleation driven growth) on secondary mineral formation and the corresponding feedback on transport properties of reference porous media. The numerical simulations presented in this study are based upon experimental dataset that investigated barite and gypsum precipitation in natural chalk sample(Rajyaguru et al., 2019). The experimental dataset were obtained based on the following principle, "fix a physical property namely pore structure heterogeneity using chalk sample and combine it with chemical property using two extremities (solubility and rate of precipitation) of sulfate alkali minerals." From this principle, it was possible to investigate the coupling effect of both properties on governing distributions of barite and gypsum mineral in the precipitation zone as well as their impact on the existing transport properties of chalk sample. The first experiment showed that barite precipitation resulted in the formation of a thin-layered clogged zone located in center of chalk sample. On the contrary, the second experiment showed that gypsum precipitation resulted in formation of isolated clusters type of clogged zone at the center of chalk sample. The water tracer tests conducted prior and after clogging phenomena showed that both of these distributions had contrasting impact on changes in chalk transport properties (with barite imparting significant reduction in tracer diffusivity compared to gypsum).

Thus, numerical description of these experimental results required a two-step approach. In the first step, using the initial and boundary conditions from experiments, barite and gypsum precipitation simulations were carried out in a homogeneous 1D geometry with total porosity of 45% (representing the mean porosity of chalk sample). The aim of these simulations was to determine the time at which precipitation is initiated, the resulting width of clogged zone and subsequent porosity reduction, and finally the evolution of chemistry evolution in reservoirs when precipitates formation modifies the pore structure of chalk sample. Indeed, at 1D, the feedback of clogged zone formation on tracers transport was simulated using empirical Archie's relationship. However, one must note that 1D simulations do not integrate spatial variability in pore size distribution of chalk sample. Thus in the second step, 2D simulations were required to accommodate this property, where pore size distribution of chalk was mimicked by integrating variable porosity (45%± 5%) while keeping the initial boundary and chemical conditions same as of 1D simulations. Since, one cannot fully resolve Archie's relationship in 2D (Deng et al., 2021), the objective of the simulations in this step was to investigate underlying factors controlling changes in distributions of barite and gypsum minerals.

157157

2 Numerical methods

2.1 Governing equations for numerical modeling

The generalized equation for modeling at REV-scale in HYTEC is well described in(Cochepin et al., 2008; Lagneau, 2013; Lagneau and van der Lee, 2010). The kinetic rate equation to model experimentally observed barite or gypsum reacted zones in chalk is described in equation-1.

$$r_s = -A_{bulk} k_{rate} \left[1 - \left(\frac{Q_s}{K}\right)\right] \quad (1)$$

where, Q_s: ion activity product, and K: mineral equilibrium constant. The bulk surface area A_{bulk} represents the overall surface over which precipitation can occur. It is the combination of the precipitation over the existing pore walls as well as a growth on barite/gypsum nuclei. These bulk surface areas can be derived from the specific surface area A_s using Equation-2

$$A_{bulk}(m^2.m^{-3}_{solution}) = A_{s,pm}C_{\mathrm{pm}} + A_{s,\mathrm{min}}C_{\mathrm{min}} \quad (2)$$

168168

or $$As = 3/\rho r \quad (3)$$

where, ρ: particle density, *r:* radius of spherical particle, *C:* Particle concentration (g/L). Hence, an initial reactivity of the porous medium is described using an unreactive mineral, with an uniform concentration (C_{pm}=1g/L) and a specific surface area of $A_{s,pm}$ = 1 m²/g, in line with literature data(Hjuler and Fabricius, 2009; Røgen and Fabricius, 2002). Then, reactivity evolves as precipitation proceeds and provides an increasing value for the bulk surface area due to evolution of C_{min}. This description is similar to the one used by (Noiriel et al., 2021).

The feedback impact of clogging on diffusivity is modeled using modified Archie's law as represented in equation 4(van der Lee et al., 2003)

$$D_e(\omega) = D_e(\phi_0)\left(\frac{\phi - \phi_c}{\phi_0 - \phi_c}\right)^{\alpha} \quad (4)$$

where D_e: effective diffusion coefficient, ϕ_c: percolation threshold, α: cementation factor

2.2 Numerical Modeling

2.2.1 1D simulations to model reacted zone

The 1D simulations were carried out to mimic counter diffusion setup used in the experiments of (Rajyaguru et al., 2019). The geometry consists of two 1 mm reservoirs sandwiching a chalk sample of uniform porosity 45% and thickness of 6.7 mm. In the experiments, the actual reservoir volumes were 178 ml for $BaCl_2$/$CaCl_2$ reservoirs and 138 ml for Na_2SO_4 reservoirs. In numerical, inserting such large volumes at boundary would result very large simulation time Thus, a bypass technique is used where 1 mm numerical reservoirs are created with porosities equal to 187 for Ca^{2+}/Ba^{2+} reservoir and 145 for SO_4^{2-} reservoir. This trick yields the correct volume (and contents in solutes) while maintaining a short distance and maximizing diffusion between the reservoirs and the chalk sample. The sample in 1D simulations was discretized with dx = 100 µm. To initiate the counter diffusion, the initial chemical conditions in each reservoirs were derived from experimental conditions (**Table-S1 in Supporting information)**. The modeling process starts by allowing these ionic species to counter diffuse and meet in the sample pore space. Over time, these ions locally increase supersaturation in pore solution with respect to barite or gypsum. Experimentally, the supersaturation state required to initiate precipitation is 4.0 for barite (Prasianakis et al.,

2017) and 0.3 for gypsum. Over time, the precipitation initiation only takes places in points that achieved this supersaturation threshold (Kashchiev and van Rosmalen, 2003; Prieto, 2014), for which Equation (1) is used. In HYTEC, initiation of first precipitates is achieved using a kinetic rate law that represents homogeneous nucleation in the entire sample by spraying the system with a pseudo-mineral "nucleus" (concentration C_{pm}) of low reactive surface area ($A_{s,pm}$). Once the supersaturation in first line of precipitation is achieved, the nucleus will allow initiation of selected mineral precipitation. Nevertheless, at the beginning of experiment if a mineral is present in a system then precipitation will occur (possibly under kinetic control) as soon a saturation is reached (saturation index ≥ 0). The values of the kinetic rate constant (k_{rate} in $mol\ m^{-2}\ s^{-1}$) and specific surface area ($A_{s,min}$ in $m^2\ g^{-1}$) for barite and gypsum equal to $k_{rate\_barite} = 1 \times 10^{-11}$; $k_{rate\_gypsum} = 1.5 \times 10^{-6}$ and $A_{s\_barite} = 0.32$ and $A_{s\_gypsum} = 1.65$ were initially derived from literature (Nagaraja et al., 2007; Potgieter and Strydom, 1996; Zhang and Nancollas, 1992). During simulations, these base values were slightly calibrated to improve the match with experimental results. In the experimental results, the diffusion behavior of ionic species from respective reservoirs into the sample were measured by periodic concentration acquisition from beginning until 140th day of experimental time. Similar concentration curves were obtained via 1D simulations and were compared with experimental results to obtain an insight on how diffusion behavior of each species changes in response to evolving precipitation in chalk sample. Similarly, tracer tests were modeled from 0 to 70 days and 70 to 140 days to estimate the precipitation feedback on chalk transport properties at different times. This feedback effect in 1D simulations were modeled using equation-4.

Sensitivity analyses were carried out to test the impact of, (1) the mesh size, by decreasing it from 100 µm, to 50 and 25 µm, (2) the cementation factor on evolution of reacted zone, with values varying from 1.5 to 2.1 and (3) the supersaturation values used to initiate the gypsum or barite precipitations. The results of each sensitivity test are presented in **Supporting Information**.

2.2.2 2D simulations

In these simulations, the initial concentration conditions of reactants in respective reservoirs and boundary conditions were kept identical as 1D simulations. However, the system in y-direction is increased up to 8 mm high with discretization as 100 µm along x- and y-axis. Similar to the 1D simulations, the reservoirs are described with porosity greater than one, to account for a larger volume, without having to resort to a too high number of nodes.

As noted in previous section, the 1D base simulations for both barite and gypsum case were modeled using a homogeneous porosity distribution in chalk sample. The kinetic rate equation used to model evolution of reacted zone uses saturation indexes that purely depend upon thermodynamic solubilities derived for bulk systems. As explained in the introduction section, the aim of this study is to demonstrate the combined effect of pore geometry (pore-scale diffusion, pore pressure, reactive surface area) and mineral intrinsic properties (solubility, precipitation rate, nucleation driven growth). However, to quantify each of these parameters one needs quantified dataset explaining local dynamics of precipitates formation, nucleation kinetics and detailed pore size distribution(Rajyaguru et al., 2019).

However, the choice of experimental setup and measurements techniques posed restriction on obtaining such local dynamic processes. Moreover, experimental observations have clearly shown a two-dimensional regime of precipitation, which cannot be represented by 1D simulations. Thus, 2D simulations were carried out and the end-results are compared with micro-tomographic images of clogged area formed by barite and gypsum in chalk samples. The aim of such comparison was to explain quantitatively the underlying processes governing global distribution of precipitates in the clogging area. To obtain a broader understanding of such underlying processes, simulations were performed using different approaches. First, 2D simulations were performed by using a non-uniform reactivity of the porous medium to account for varying reactive surfaces initially present in chalk sample and their impact on governing distributions of barite and gypsum in clogging area (non-uniform distribution of C_{pm}). Then, heterogeneous distribution of porosities was considered to describe impact of local variation in diffusion of ionic species. Two cases were considered: a initial purely random Gaussian heterogeneous porosity field (Fig. 1a) and a structured heterogeneous porosity field (Fig. 1b). Third, different kinetic scenarios were investigated to disentangle the nucleus-driven nucleation vs a crystal-growth nucleation (Table 1). A direct comparison of barite and gypsum distributions in latter case allowed us to derive the porosity field that closely mimicked pore structure of natural chalk used in the experimental study of (Rajyaguru et al., 2019). Finally, comparing results of both cases with experimental observations allowed us to demonstrate whether pore structure heterogeneity controlled transport local ionic species diffusion or generating varying reactive surface was responsible for distinct distribution of gypsum and barite in the chalk sample.

Figure-1 shows two representative porosity fields accounting for purely random heterogeneity and structured heterogeneity. As shown in Figure1A, the first random porosity field was generated without spatial structure with a normal distribution centered on 0.45, with a standard deviation 0.05. The end results of simulations obtained using such random heterogeneous porosity field provide us a good starting point to inspect as whether initial presence of surface sites reactivity or pore structure heterogeneity had a pronounced impact on controlling distributions of barite and gypsum in chalk sample. However, one must note that the pore structure of natural chalk sample is formed via breaking down of algae known as coccolithophore into calcite grains. Depending upon the burial depth, the heterogeneity of pore structure in chalk sample consists of macropores stemming from coccolithophores and microporosity between void spaces of calcite grains. Several studies focusing on petrophysics of natural chalk have shown that such heterogeneities could be decomposed into statistically representative elementary volumes ($SREV^s$) of correlation lengths ranging from 5 µm to 100 µm (Bruns et al., 2017; Müter et al., 2014; Villanova et al., 2013). Nevertheless, as formation of chalk pore structure purely depends on the nature of sedimentation process and burial depth, these correlation lengths of $SREV^s$ could significantly vary for same family of micritic chalk at different burial sites (Faÿ-Gomord et al., 2017; Yoon and Dewers, 2013). In the present study, such correlation lengths could be used to demonstrate if representation of a REV in form of such structured heterogeneities could result in closer prediction of barite and gypsum distributions in chalk samples. In this view, a second random porosity field shown in Figure-1B was generated with the same mean and deviation as purely random case, but integrating a spatial structure with a correlation length of 100 µm; the porosity field was simulated using the geostatistics library RGeostats (Renard et al., 2015). For both cases, the counter diffusion geometry, initial Ca/Ba and SO_4 reservoir

285 concentrations, diffusive coefficients, kinetic rate constants and specific surface area were
286 kept similar to 1D simulations.

287287

288 Table 1: Input parameters for kinetic rate expressions: chalk reactivity ($A_{s,pm}$ in $m^2.g^{-1}$), and mineral
289 surface area (A_{gypsum} and A_{barite} in $m^2.g^{-1}$) and supersaturation (SI) used for gypsum and barite growth
290 in subset nucleus driven and transport driven growth.

Case	$a_{S,pm}$	$A_{S,Gypsum}$	SI_{GYPSUM}	$A_{S,Barite}$	si_{barite}
Nucleus driven growth	1	0.1	0.3	1.8	4
Nucleus driven growth	100	0.1	0.3	1.8	4
Transport driven growth	1	10	0.3	1.8	4

291291

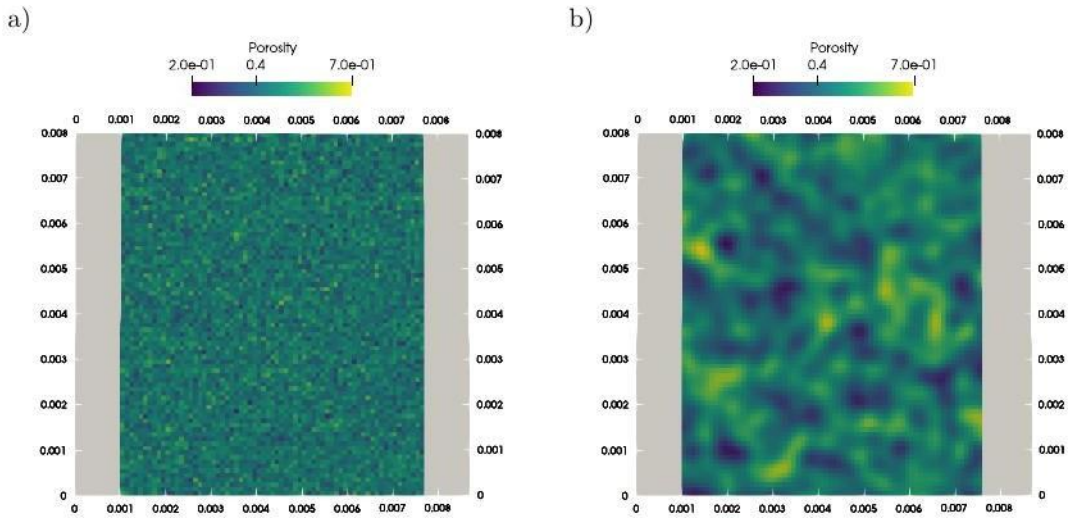

292292

293 Figure 1: Random porosity fields used in the 2D simulations. A: purely random unstructured gaussian
294 porosity field with mean 45% and std 5%. B: random gaussian porosity field with a correlation length
295 of 100 µm.

296296

297 3 Results and discussion

298 3.1 Barite Base Simulation

299 The 1D simulation results for barite precipitation and its feedback impact on tracer diffusivity
300 are presented in Figure 2 with a comparison to experimental results from (Rajyaguru et al.,
301 2019). As the simulation starts, the reactants diffuse into the chalk sample and decrease the
302 ionic concentrations in the reservoir (Figure 2e). Consequently, Figure 2a shows a simulated
303 diffusion profile for Ba^{2+} and SO_4^{2-} from each side of chalk surface towards the center of the
304 sample. Over the simulation time, Ba^{2+} and SO_4^{2-} ions meet in the center of the chalk sample
305 and increase the saturation of pore solution with respect to barite mineral. Once the
306 threshold super-saturation is achieved, barite precipitates locally. Owing to the very low
307 solubility product for barite, the simulations show that barium and sulfate concentrations are
308 kept very low within the precipitation zone. The simulations further show that most of the
309 barite precipitates grow in this first line of precipitation and the resulting clogging front
310 evolves in a thin zone (Figure 2c). A progressive porosity loss and consequent diffusivity
311 decrease (Figure 2b and 2d, resp.) is evidenced in this clogging zone. Indeed, as the size of
312 clogging zone starts to become significant, a clear feedback on porosity and diffusivity loss is
313 observed on Ba^{2+} and SO_4^{2+} concentration profiles in the reservoir (Figure 2a). After 50 days,
314 the diffusive barrier created by the barite layer isolates the two reservoirs, consequently
315 limiting any further precipitation process. This was observed experimentally with barium
316 concentration reaching quasi-equilibrium state (Figure 2e). At this stage, using the initial and
317 final concentration, it is possible to estimate the contribution of Ba^{2+} to barite precipitation in
318 chalk sample. The simulations predicted that 2.7 mol of Barite precipitated in chalk sample.
319 This estimate was well in accordance with experimental estimated barium contribution to
320 barite precipitation, *i.e.* 2.5 mol "for detailed calculation refer to (Rajyaguru et al., 2019)". At
321 the end of the simulations, the predicted final thickness of clogging zone (highlighted in

orange in Figure 2f) is equal to ~600 µm (which is close to ~500 µm barite zone in chalk sample observed by BSE-SEM images in (Rajyaguru et al., 2019)). To estimate the feedback of barite precipitation on diffusion, water tracer tests performed at 0 days and 70 days after the start of the clogging experiment. However, Figure 2f shows that the numerical simulations slightly underestimated the reduction in tracer profile for the case of 0 to 70 days and slightly overestimated the reduction in tracer profile for 70 to 140 days. This small contradiction between experimental and numerical results is due to the fact that in real sample the impact on tracer transport occurred due to the occurrence of clogging phenomena in a 3D-heterogeneous pore structure, whereas the numerical simulations calculated the tracer profiles based upon the total porosity loss at 1D using Archie's relationship. One must note that the results presented in supporting information for sensitivity of mesh size and cementation factor reveals a limited impact of these parameters on the final outcomes of 1D simulations. Conversely, kinetic rate and chalk initial reactive surface area exhibit a larger control on simulation results.

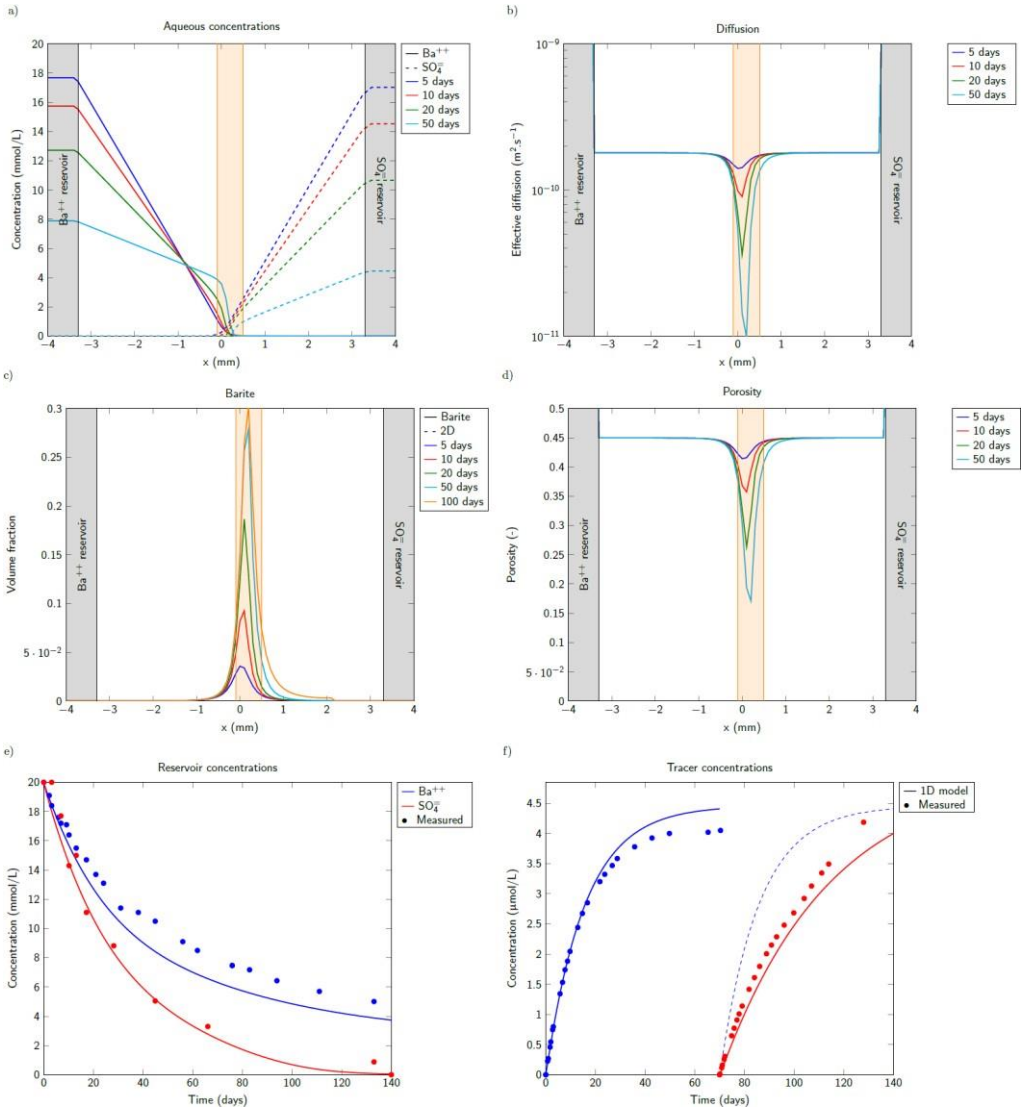

Figure 2: comparison between HYTEC and experimental data for chalk barite simulation. **A**: concentration profiles for Ba^{2+} and SO_4^{2-} at 5, 10, 20 and 50 days, **B:** evolution of the effective

diffusion coefficient, **C**: barite volume fraction profiles, **D**: evolution of porosity **E:** Evolution of reservoir concentrations for Ba^{2+} and SO_4^{2} and comparison between models (1D & 2D) with measured values (circles), **F**: Experimental (circles) and numerical (continuous line) water tracer evolution in downstream reservoirs for water tracer injected at 0 days and 70 days after barite precipitation. One must note that the dashed line represents a translation of the initial blue model line, and orange zone represents central zone of the chalk sample.

3.2 Gypsum Base Simulation

3.2.1 1D simulation

Figure 3, represents the 1D numerical results for gypsum precipitation in chalk sample. The simulations show that as Ca^{2+} and SO_4^{2-} diffuse into the chalk sample, a progressive increase in the saturation with respect to gypsum is observed in the center of the sample (figure 3b). The concentration profiles of Ca^{2+} and SO_4^{2+} (Figure 3a & 3e) show that each of the ion diffuses from their respective reservoirs into the chalk sample and then into the counter reservoir. These figures show an increase in Ca^{2+} and SO_4^{2-} concentration in counter reservoirs for initial 20 days, after which their concentration reach a quasi-equilibrium state for 140 days of experimental time. Such increase in their concentration resulted in small precipitation of gypsum in both reservoirs. The numerical simulations were able to reproduce these experimentally observed concentration profiles and hinted towards gypsum precipitation in reservoirs (Figure 3c). This is marked by the discontinuity in the reservoir concentration curves (Figure 3e), which occurs when supersaturation to initiate precipitation is reached in the reservoir. As a result, their diffusion profiles are very different compared to the barite case (compare Figure 3a to Figure 2a). Unlike barite, gypsum is a fairly soluble mineral, so that the pore solution requires more calcium and sulfate ions to reach the saturation threshold to initiate precipitation. Consequently, longer times are required to achieve such saturation values that could initiate precipitation and form a strong clogging zone capable of restricting the diffusion Ca^{2+} and SO_4^{2-} ions into the counter reservoir. However, once the precipitation starts a progressive increase of gypsum mineral in the chalk sample takes place (Figure 3c). Similar to barite case, the impact of gypsum precipitation on chalk sample was estimated by tracer tests performed at 0 days and 70 days and 70 to 140 days after the start of the clogging experiment. The corresponding numerical results presented in Figure 3f shows that the numerical simulations reproduced the tracer profile for the case of 0 to 70 days, but clearly underestimated the tracer profile for 70 to 140 days. This limitation of 1D simulations to describe the impact of gypsum clogging on chalk transport properties clearly suggests that small-scale heterogeneity either in reactive surface area or in transport properties is likely to have a pronounced impact on distribution of precipitates, width of the clogging area and feedback on tracer diffusivity. Indeed, a direct comparison between Figure 3c and Figure 2c shows that even at 1D scale the final width of clogging zone is strongly dependent on the ratios between, solubility, precipitation kinetics and transport properties. Thus, to describe properly the barite and gypsum clogging in chalk samples it is imperative to perform numerical simulation with similar initial and boundary conditions as 1D scale but now taking into account the pore scale heterogeneities. For such approach, one needs to move from 1D scale to 2D scale.

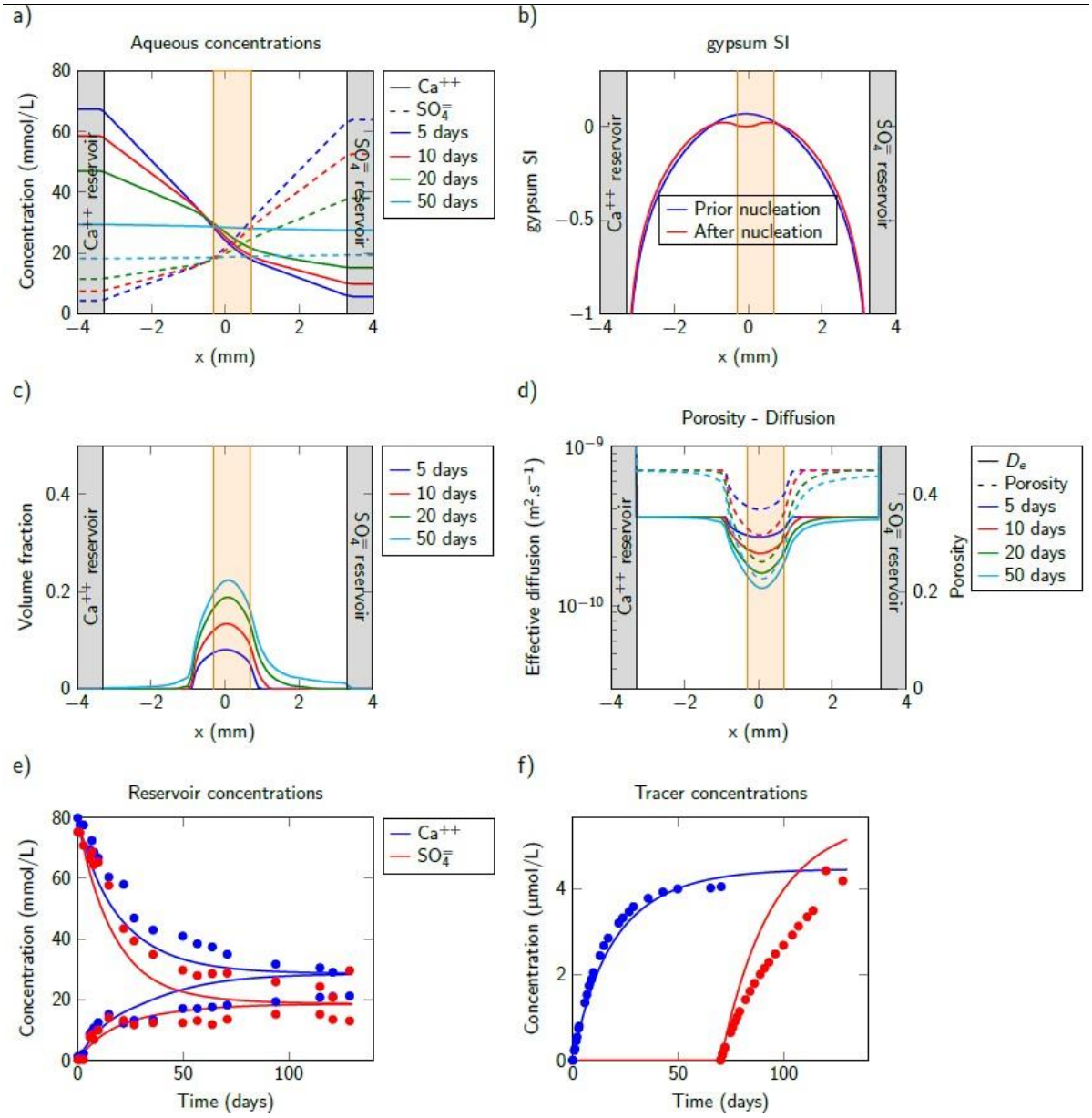

Figure 3: comparison between HYTEC and experimental data for basic chalk gypsum simulation, A: Concentration profiles of Ca^{2+} (solid lines) and SO_4^{2-} (dashed lines) **B**: gypsum saturation index at 5, 10, 20 and 50 days in the precipitation zone, **C:** gypsum volume fraction profile in the sample and in the reservoirs, **D**: porosity loss due to gypsum precipitation and its impact on local diffusivity reduction in the center of the sample, **E**: Experimental (circles) and numerical (continuous line) concentration evolution of SO_4^{2-} and Ca^{2+} in their respective reservoirs for total experimental time of 140 days, **F**: Experimental (circles) and numerical (continuous line) water tracer evolution in downstream reservoirs for water tracer injected at 0 days and 70 days after gypsum precipitation. One must note that the orange zone represents central zone of the chalk sample where most of the clogging occurred during precipitation process.

3.2.2 2D simulations

At first, gypsum simulations were performed using a varying reactivity of the porous medium within the chalk sample (Fig 4a) and using a purely random porosity field (Fig 4b). Fig 4a

shows that presence of such reactive sites does not yield a final distribution of gypsum precipitation that is comparable to experimental results (see figure S4 in **supporting information)**. Indeed, the location of nucleation control depends on where supersaturation is reached, which does not depend on reactivity. As further precipitation is dominated by the growth of gypsum, the precipitation front is very similar to the one observed for 1D simulations. Also, a purely random porosity field does not yield strong differences, as the lack of structure averages out the different path and yield a similar precipitation pattern (Fig 4b).

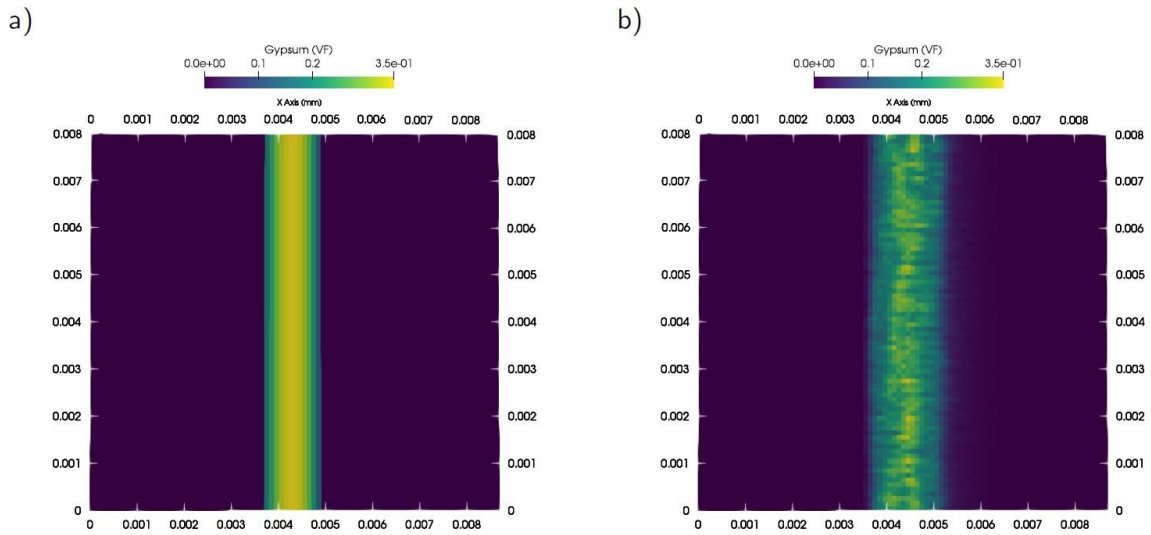

Figure 4: Distribution of Gypsum precipitation for two scenarios at the end of simulation time of 140 days. a) Homogeneous porosity with varying reactivity of the porous medium. b) Purely random porosity field.

Conversely, using a porosity distribution exhibiting a certain degree of structure allows some locations to initiate precipitation before others and thereby leading to formation of a discontinuous zone of precipitation with certain clusters. The numerical simulation did show such behavior on formation of isolated clusters of gypsum (Fig. 5 a) and which is in very good visual agreement with tomographic images that are presented in figure S4 in **supporting information**. Based on these simulations, it seems that the appearance of clusters is dependent on the combined effect of relative rates of transport and reaction kinetics. Furthermore, the influence of nucleation kinetics on gypsum precipitation is illustrated in Figure-6. Figure-6a shows that nucleation driven kinetics leads to discrete spots of precipitation, while Figure-6b shows that growth-driven kinetics yields thin precipitation zone.

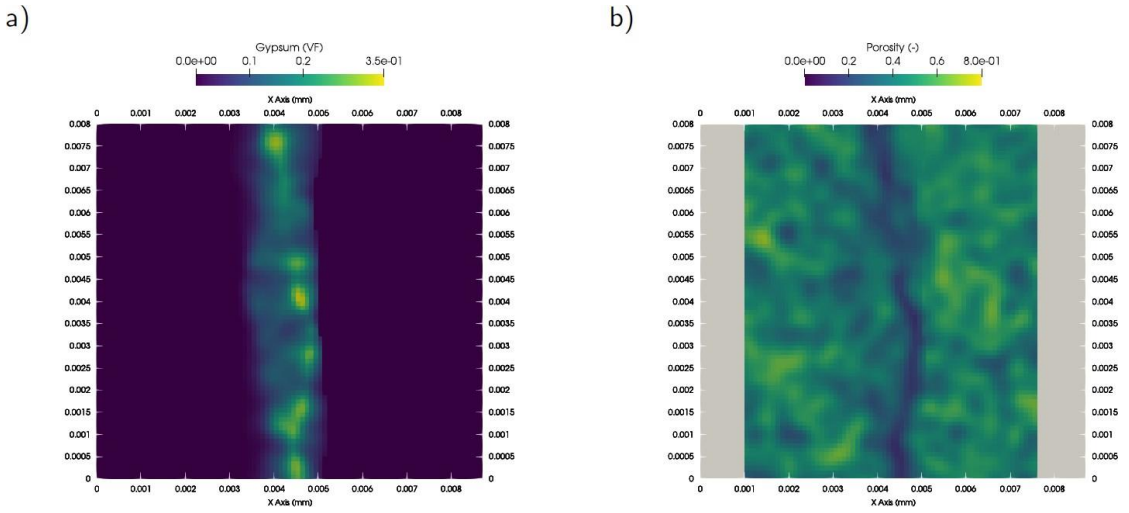

419419

420 Figure 5: Final distribution of gypsum and associated porosity reduction for 2D simulations. Porosity
421 of the reservoirs (above 1) is excluded from the color scale.

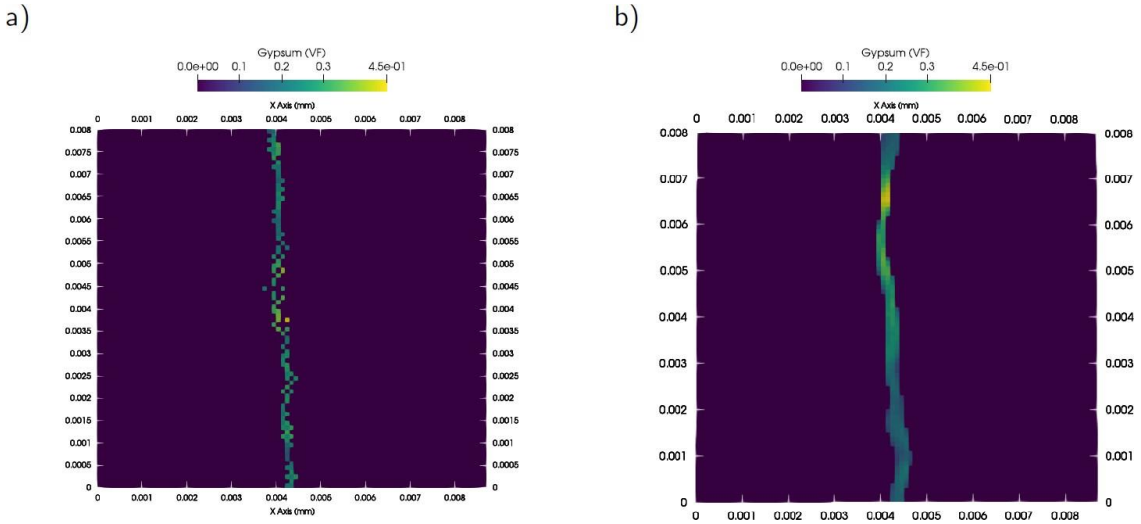

422422

423 Figure 6: Influence of the nucleation mode. A) Nucleation driven precipitation modelled by a high
424 initial porous medium reactivity. B) Gypsum-growth mechanism. One must note that the presented
425 precipitation patterns were obtained at the end of simulation time of 140 days

426426

427 ## 3.3 Barite simulation with spatial variability

428 We have shown that, for the gypsum case, incorporating a structured porosity field was
429 required. One may wonder as what are the impacts of considering these pore-scale
430 heterogeneities for the barite simulation. The results presented in Figure 7, shows a cross-
431 section view of 2D barite simulation carried out in the two random heterogeneous porosity
432 fields (with and without structure). In both cases, barite precipitation is confined within a thin
433 zone in the center of the sample. Simulation suggests a significant porosity loss within the
434 clogged zone in the porous medium at the end of the experiment (Figure 7). Both
435 simulations display similar formation of a thin, continuous and regular, barite-clogged area.
436 Comparison of both simulations confirms that for the barite experiment, spatial variability

triggers small local variations in the diffusion of reactants towards the center of the sample; however, due to the low solubility of barite, the supersaturation to initiate precipitation is similar to the (1D) homogeneous base case. The slow kinetics further compensated the impact of local variation in selective precipitation initiation preventing the scenario of spheres formation. As simulations proceeds, barite grows at these first points of precipitates in the center of the sample. Nevertheless, one could clearly observe that the clogged zone formation using of structured porosity field produce barite distributions closer to experimental results (refer to Figure S5 in Supporting information).

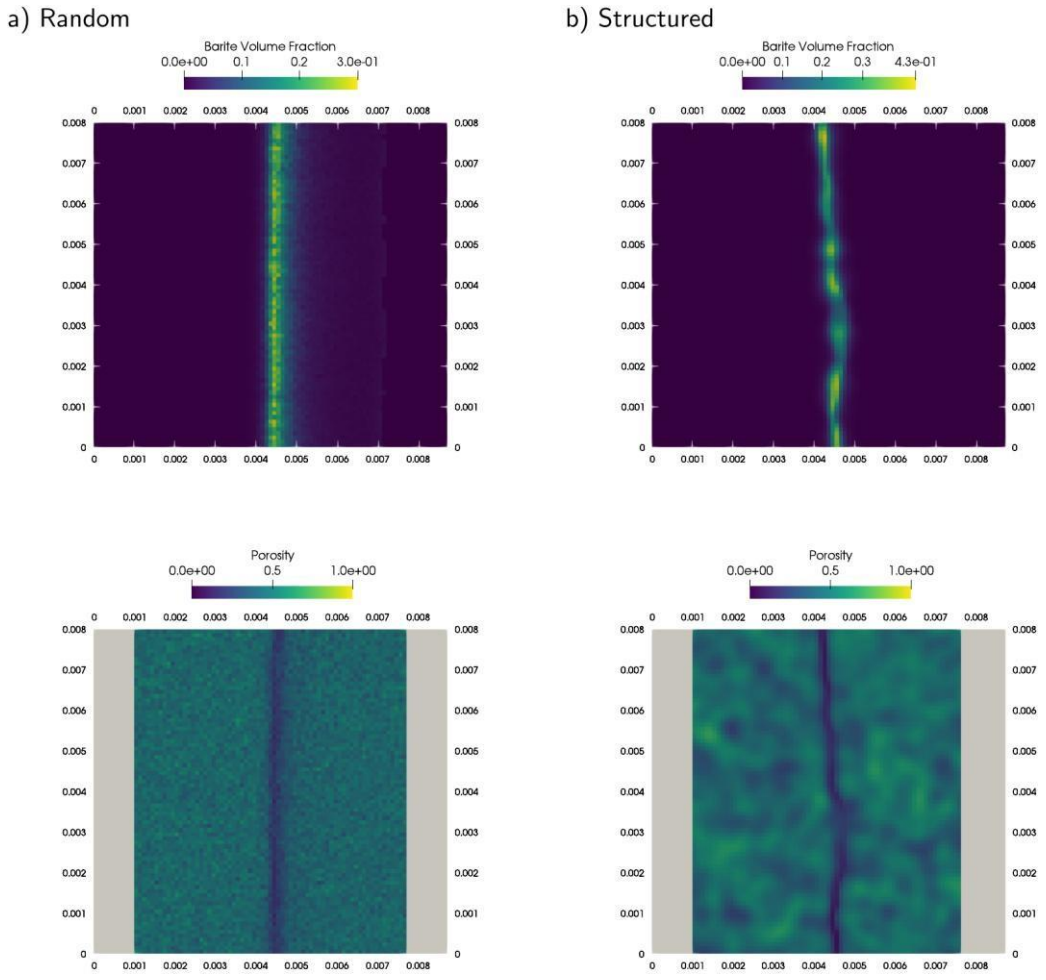

Figure 7: evolution of barite volume fraction (top) and porosity field (bottom) mineral using HYTEC at the end of the simulation (140 days).

4 Conclusion:

In this study, two sets of numerical simulations were performed to investigate coupled impact of physical properties in the form of pore structure heterogeneity with chemical properties in the form of mineral intrinsic properties (solubility, rate kinetics) in driving distribution and porosity loss via secondary mineral formation. The 1D modeling results derived crucial information on location of clogged area, total porosity loss and mass transfer from inlet

reservoirs to sample. For barite precipitation in chalk, the experiments showed the formation of clogging zone a thin layered structure and was located at the center of the sample. At 1D, it was possible to reproduce this clogging feature using numerical simulations and with correct estimation of Ba^{2+} and SO_4^{2-} diffusion from sample boundary, overall amount of barite precipitation in the sample, and fair estimation of feedback on water tracer diffusivity. Thus, these simulations show that for some mineral such as barite, 1D simulations are useful to derive the processes at boundary conditions. For gypsum experiments, the numerical simulations fairly determined the Ca^{2+} and SO_4^{2-} diffusion from sample boundary. The simulations also correctly hinted towards diffusion of ions into the counter reservoirs and contributing to precipitation at bulk conditions. However, in this case Archie's relationship clearly underestimated the tracer transport after formation of clogging zone. Nevertheless, both barite and gypsum experiments clearly hinted towards performing numerical simulations where clogging behavior could be modeled by taking into account the presence of small-scale structured heterogeneities that could not be resolved in 1D via sensitivity analysis by changing parameters such kinetic rate, cementation factor, mesh size and saturation index values. In this view, the first set of numerical simulations at 2D scale considered investigating precipitates distribution and local porosity loss in response to structured and unstructured random porosity fields. However, the second set of numerical simulations considered investigating the formation of clogging zone in a chalk sample that initially contains randomly sprayed reactive surfaces. In the former case, the aim of simulations was to investigate the competition between mass transport and reaction kinetics, and in latter case, the aim of simulations was to generate a competition between kinetic driven and nucleation growth precipitation. The results of both simulations exercise showed that the consideration of structured heterogeneous porosity field showed gypsum distribution very similar to experimental results. These findings clearly validate the assumption presented in (Rajyaguru et al., 2019), *i.e.* "gypsum precipitation behavior in chalk is due to strong coupling between reaction kinetics and pore structure heterogeneity." However, the simulations results for barite conducted for purely random and structured porosity field showed a thin layered clogging front in the center of the sample. This observation clearly hints towards the fact that barite precipitation is indeed growth dependent. Thus, the numerical simulations presented in this study provide an essential information pertaining to the choice of scale that is necessary for studying clogging in porous media. A key information that could be derived from this exercise is the need to develop dedicated experimental datasets and test them using pore-scale modelling. It is imperative that the strong coupling of such experimental and numerical exercises could only derive the novel feedback relationship replacing Archie's relationship.

Finally, from 1D and 2D experimental results, we conclude that reactive transport simulations enabled to validate the model based on experimental results presented in (Rajyaguru et al., 2019), *i.e.* "how the physicochemical processes at stake yielded such different precipitation morphologies." In the end, the understanding obtained by the reactive transport approach allows to draw conclusions that may be suited to other types of simulations with geoengineering relevance.

500500

501501

502502

503503

504504

505 References

506 Archie, G.E., 1942. The Electrical Resistivity Log as an Aid in Determining Some Reservoir
507 Characteristics. Trans. AIME 146, 54–62. https://doi.org/10.2118/942054-G

508 Bear, J., 2013. Dynamics of fluids in porous media. Courier Corporation.

509 Berkowitz, B., Cortis, A., Dentz, M., Scher, H., 2006. Modeling Non-fickian transport in
510 geological formations as a continuous time random walk. Rev. Geophys. 44, 1–49.
511 https://doi.org/10.1029/2005RG000178

512 Berthe, G., 2012. Évolution des propriétés de confinement des roches-couvertures type
513 argilite soumises à des fluides enrichis en CO2: impact des discontinuités naturelles et
514 artificielles. Université Paris Sud-Paris XI. Francais. NNT : 2012PA112420. tel-
515 00795668.

516 Bradbury, M.H., Berner, U., Curti, E., Hummel, W., Kosakowski, G., Thoenen, T., 2014. The
517 long term geochemical evolution of the nearfield of the HLW repository. Paul Scherrer
518 Institute (PSI).

519 Bruns, S., Stipp, S.L.S., Sørensen, H.O., 2017. Statistical representative elementary
520 volumes of porous media determined using greyscale analysis of 3D tomograms. Adv.
521 Water Resour. 107, 32–42.

522 Carman, P.C., 1937. Fluid flow through granular beds. Trans. Inst. Chem. Eng. 15, 150–166.

523 Cochepin, B., Trotignon, L., Bildstein, O., Steefel, C.I., Lagneau, V., Van der lee, J., 2008.
524 Approaches to modelling coupled flow and reaction in a 2D cementation experiment.
525 Adv. Water Resour. 31, 1540–1551. https://doi.org/10.1016/j.advwatres.2008.05.007

526 Deng, H., Tournassat, C., Molins, S., Claret, F., Steefel, C.I., 2021. A Pore-Scale
527 Investigation of Mineral Precipitation Driven Diffusivity Change at the Column-Scale.
528 Water Resour. Res. 57, e2020WR028483.

529 Faÿ-Gomord, O., Soete, J., Davy, C.A., Janssens, N., Troadec, D., Cazaux, F., Caline, B.,
530 Swennen, R., 2017. Tight chalk: Characterization of the 3D pore network by FIB-SEM,
531 towards the understanding of fluid transport. J. Pet. Sci. Eng. 156, 67–74.
532 https://doi.org/10.1016/j.petrol.2017.05.005

533 Glaus, M.A., Frick, S., Van Loon, L.R., 2020. A coherent approach for cation surface
534 diffusion in clay minerals and cation sorption models: Diffusion of Cs+ and Eu3+ in
535 compacted illite as case examples. Geochim. Cosmochim. Acta 274, 79–96.

536 Hjuler, M.L., Fabricius, I.L., 2009. Engineering properties of chalk related to diagenetic
537 variations of Upper Cretaceous onshore and offshore chalk in the North Sea area. J.
538 Pet. Sci. Eng. 68, 151–170. https://doi.org/10.1016/j.petrol.2009.06.005

539 Jun, Y.S., Giammar, D.E., Werth, C.J., 2013. Impacts of geochemical reactions on geologic
540 carbon sequestration. Environ. Sci. Technol. 47, 3–8.
541 https://doi.org/10.1021/es3027133

542 Kashchiev, D., van Rosmalen, G.M., 2003. Review: Nucleation in solutions revisited. Cryst.
543 Res. Technol. 38, 555–574. https://doi.org/10.1002/crat.200310070

544 Lagneau, V., 2013. Modélisation des couplages entre réactions géochimiques et processus
545 hydrodynamiques en milieu poreux – applications au stockage de CO 2 et à
546 l'exploitation d'uranium. Géochimie. Université Pierre et Marie Curie - Paris VI, 2013.
547 tel-00879817.

548 Lagneau, V., van der Lee, J., 2010. Operator-splitting-based reactive transport models in
549 strong feedback of porosity change: The contribution of analytical solutions for accuracy
550 validation and estimator improvement. J. Contam. Hydrol. 112, 118–129.
551 https://doi.org/10.1016/j.jconhyd.2009.11.005

552 Landesman, C., Macé, N., Radwan, J., Ribet, S., Bessaguet, N., David, K., Page, J.,
553 Henocq, P., 2018. Effect of high saline alkaline conditions onto radionuclide transport in
554 a CEM V/A hardened cement paste, in: NUWCEM, Cement-Based Materials for
555 Nuclear Waste.

556 Lasaga, A.C., 2014. Kinetic theory in the earth sciences. Princeton university press.

557 Moldovan, B.J., Jiang, D.T., Hendry, M.J., 2003. Mineralogical characterization of arsenic in
558 uranium mine tailings precipitated from iron-rich hydrometallurgical solutions. Environ.
559 Sci. Technol. 37, 873–879. https://doi.org/10.1021/es025947a

560 Müter, D., Sørensen, H.O., Jha, D., Harti, R., Dalby, K.N., Suhonen, H., Feidenhans'l, R.,
561 Engstrøm, F., Stipp, S.L.S., 2014. Resolution dependence of petrophysical parameters
562 derived from X-ray tomography of chalk. Appl. Phys. Lett. 105, 43108.

563 Nagaraja, B.M., Abimanyu, H., Jung, K.D., Yoo, K.S., 2007. Preparation of mesostructured
564 barium sulfate with high surface area by dispersion method and its characterization. J.
565 Colloid Interface Sci. 316, 645–651. https://doi.org/10.1016/j.jcis.2007.09.004

566 Noiriel, C., Seigneur, N., Le Guern, P., Lagneau, V., 2021. Geometry and mineral
567 heterogeneity controls on precipitation in fractures: An X-ray micro-tomography and
568 reactive transport modeling study. Adv. Water Resour. 152, 103916.

569 Nooraiepour, M., Masoudi, M., Hellevang, H., 2021. Probabilistic nucleation governs time,
570 amount, and location of mineral precipitation and geometry evolution in the porous
571 medium. Sci. Rep. 11, 1–17.

572 Potgieter, J.H., Strydom, C.A., 1996. An investigation into the correlation between different
573 surface area determination techniques applied to various limestone-related compounds.
574 Cem. Concr. Res. 26, 1613–1617. https://doi.org/10.1016/S0008-8846(96)00159-7

575 Prasianakis, N.I., Curti, E., Kosakowski, G., Poonoosamy, J., Churakov, S. V., 2017.
576 Deciphering pore-level precipitation mechanisms. Sci. Rep. 7, 1–9.
577 https://doi.org/10.1038/s41598-017-14142-0

578 Prieto, M., 2014. Nucleation and supersaturation in porous media (revisited). Mineral. Mag.
579 78, 1437–1447. https://doi.org/10.1180/minmag.2014.078.6.11

580 Rajyaguru, A., L'Hôpital, E., Savoye, S., Wittebroodt, C., Bildstein, O., Arnoux, P., Detilleux,
581 V., Fatnassi, I., Gouze, P., Lagneau, V., 2019. Experimental characterization of coupled
582 diffusion reaction mechanisms in low permeability chalk. Chem. Geol. 503.
583 https://doi.org/10.1016/j.chemgeo.2018.10.016

584 Renard, D., Bez, N., Desassis, N., Beucher, H., Ors, F., Laporte, F., 2015. RGeostats: The
585 Geostatistical package [version: 11.0. 3]. MINES ParisTech. Free download from
586 http//cg. ensmp. fr/rgeostats.

587 Røgen, B., Fabricius, I.L., 2002. Influence of clay and silica on permeability and capillary
588 entry pressure of chalk reservoirs in the North Sea. Pet. Geosci. 8, 287–293.

589 Sabo, M.S., Beckingham, L.E., 2021. Porosity-Permeability Evolution During Simultaneous
590 Mineral Dissolution and Precipitation. Water Resour. Res. 57, e2020WR029072.

591 Seigneur, N., Mayer, K.U., Steefel, C.I., 2019. Reactive transport in evolving porous media.
592 Rev. Mineral. Geochemistry 85, 197–238.

593 Snæbjörnsdóttir, S.Ó., Sigfússon, B., Marieni, C., Goldberg, D., Gislason, S.R., Oelkers,
594 E.H., 2020. Carbon dioxide storage through mineral carbonation. Nat. Rev. Earth
595 Environ. 1, 90–102.

596 Steefel, C.I., Yang, L., 2021. Secondary magnesite formation from forsterite under CO2
597 sequestration conditions via coupled heterogeneous nucleation and crystal growth.
598 Geochim. Cosmochim. Acta 311, 29–42.

599 Steinwinder, J., Beckingham, L.E., 2019. Role of pore and pore-throat distributions in
600 controlling permeability in heterogeneous mineral dissolution and precipitation
601 scenarios. Water Resour. Res. 55, 5502–5517.

602 Thakur, J.K., Thakur, R.K., Ramanathan, A.L., Kumar, M., Singh, S.K., 2010. Arsenic
603 contamination of groundwater in Nepal—an overview. Water 3, 1–20.

604 Trinchero, P., Iraola, A., 2020. Models for the assessment of transport of naturally-occurring
605 nuclides in fractured media. J. Hydrol. 580, 124322.

606 van der Lee, J., De Windt, L., Lagneau, V., Goblet, P., 2003. Module-oriented modeling of
607 reactive transport with HYTEC. Comput. Geosci. 29, 265–275.
608 https://doi.org/10.1016/S0098-3004(03)00004-9

609 Varzina, A., Cizer, Ö., Yu, L., Liu, S., Jacques, D., Perko, J., 2020. A new concept for pore-
610 scale precipitation-dissolution modelling in a lattice Boltzmann framework-Application
611 to portlandite carbonation. Appl. Geochemistry 123, 104786.

612 Villanova, J., Laurencin, J., Cloetens, P., Bleuet, P., Delette, G., Suhonen, H., Usseglio-
613 Viretta, F., 2013. 3D phase mapping of solid oxide fuel cell YSZ/Ni cermet at the
614 nanoscale by holographic X-ray nanotomography. J. Power Sources 243, 841–849.

615 Yoon, H., Dewers, T.A., 2013. Nanopore structures, statistically representative elementary
616 volumes, and transport properties of chalk. Geophys. Res. Lett. 40, 4294–4298.

617 Zhang, J., Nancollas, G.H., 1992. Influence of calcium/sulfate molar ratio on the growth rate
618 of calcium sulfate dihydrate at constant supersaturation. J. Cryst. Growth 118, 287–
619 294. https://doi.org/10.1016/0022-0248(92)90073-R

620